MRS Communications

https://doi.org/10.1557/s43579-021-00012-4

MRS Communications

Polymers for Additive Manufacturing Prospective

Structural response of 3D-printed rubber lattice structures under compressive fatigue

Mohammad I. Hatamleh, Department of Mechanical Engineering, Erik Jonsson School of Engineering and Computer Science, The University of Texas at Dallas, 800 W. Campbell Road, Richardson, TX 75080, USA; Adaptive 3D Technologies, 608 Development Drive, Plano, TX 75074, USA
Carlos A. Barrios, Adaptive 3D Technologies, 608 Development Drive, Plano, TX 75074, USA
Yao Ren, Runyu Zhang, Visakhan Vijayan Nambiar, and **Austin Williams,** Department of Mechanical Engineering, Erik Jonsson School of Engineering and Computer Science, The University of Texas at Dallas, 800 W. Campbell Road, Richardson, TX 75080, USA
Pratik Shah, Adaptive 3D Technologies, 608 Development Drive, Plano, TX 75074, USA
Alan Guyan, Additive Accelerator, 221 Thomas Ave., Baltimore, MD 21225, USA
Benjamin Lund, Adaptive 3D Technologies, 608 Development Drive, Plano, TX 75074, USA
Hongbing Lu, Department of Mechanical Engineering, Erik Jonsson School of Engineering and Computer Science, The University of Texas at Dallas, 800 W. Campbell Road, Richardson, TX 75080, USA
Walter Voit, Department of Mechanical Engineering, Erik Jonsson School of Engineering and Computer Science, The University of Texas at Dallas, 800 W. Campbell Road, Richardson, TX 75080, USA; Adaptive 3D Technologies, 608 Development Drive, Plano, TX 75074, USA; Department of Materials Science and Engineering, Erik Jonsson School of Engineering and Computer Science, The University of Texas at Dallas, 800 W. Campbell Road, Richardson, TX 75080, USA; Center for Engineering Innovation, The University of Texas at Dallas, 800 W. Campbell Road, Richardson, TX 75080, USA

Address all correspondence to Walter Voit at **Walter.voit@utdallas.edu**

(Received 11 September 2020; accepted 3 January 2021)

Abstract

A new direct UV curing, polyurethane-like, highly stretchable rubber, Elastic ToughRubber 90™ (ETR 90), is demonstrated for 3D printing via photo-curing with Texas Instruments DLP® optical systems. An array of test specimens, comprising a sandwich structure with a body-centered cubic lattice core, are 3D printed from ETR 90. The compressive behavior of these specimens is characterized up to 10 k and up to 100 k fatigue-loading cycles. The internal, visually obstructed, structures under loads are visualized using in situ X-ray tomography. All lattice structures remain intact and full recovery is observed, indicating the cyclic durability of the 3D-printed rubber.

Introduction

The demand for elastic, tough rubber lattices has been increasing in such commercial segments as consumer (with specific applications in footwear, mattress, noise-attenuating devices), transportation (automotive interiors, rail and aerospace), oil and gas, industrial and electronic and medical devices and packaging due to the need for materials with exceptional properties including high flexibility, high tear strength, high resilience, and high tensile strength. Elastomers and rubber-like materials can sustain large deformations without failure, typically at strain capacities above 200%, and, once deformed, recover rapidly to their original dimensions.[1] Microscopically, these characteristics are the result of combining high molecular weight polymer chains with inter-chain entanglements, sometimes with covalent crosslinking, and a glass transition temperature significantly lower than their operating temperature. Above their glass transition temperatures, rubbers are amorphous and their constituent, monomeric segments change their position readily and continuously.[1] If the polymer chains are entangled or cross-linked, the chains form a loose three-dimensional molecular network with a more restricted segmental motion. Some rubbers of high-molecular-weight have a network solely consisting of highly entangled, long molecules with a spacing between entanglements being characteristic for each particular polymer; some other rubbers have chains that are chemically cross-linked, in which some of the chains form a permanent network, as is the case for vulcanized rubber. Ultimately, rubbery materials with the desired mechanical properties can be engineered by balancing molecular weight, chain entanglements, crosslinking density and reinforcing fillers. Previous studies investigated the ability to use rubbers in 3D printing. Lukić et al. investigated the feasibility of 3D printing of a latex material including natural rubber and prevulcanized natural rubber using inkjet printing.[2] The surface tension, viscosity and particle size were measured. Scott et al. designed and created a photopolymer and a vat photopolymerization (VP) system for additive manufacturing,[3] with which they were able to print a styrene-butadiene rubber (SBR).

In this study, ETR 90, a high-strain polyurethane-like elastomer, was photo-patterned by a Texas Instruments DLP® based projector with a UV (385 nm) light source. ETR 90 was used to additively manufacture lattice structures; their mechanical behavior depends on such parameters as relative density, material properties, unit cell topologies and strut thickness.[4] A number of lattice structures, including unit-cells such as the octet, gyroid, face-centered cubic, body-centered cubic, etc.,

have been used in engineering applications to tune such properties as density, energy absorption, stiffness, resilience and strength[5, 6] Ling et al. studied experimentally and numerically the mechanical behavior and energy absorption of different relative density 3D printed polymeric octet-truss lattice structure under static and dynamic compression. In that work, two different polymer resins from Formlabs were studied, the *standard grey* and *durable* resins, respectively. The 3D printed *durable* sample demonstrated greater energy absorption compared to the *standard grey* 3D printed sample. Under dynamic impact loading, the 3D printed *durable* sample showed a strain-rate strengthening effect while the converse, a strain-rate weakening effect, was observed for the *standard grey* resin specimen.[5] Yu et al. studied a series of 3D-printed, self-healing polymers printed into lattice structures. Self-healing was triggered by fracture and shape-memory effects. The effect of 3D-printed lattice structure, including honeycomb and octet, on the polymer's healing ability was found to be minimal.[6]

In this paper, a body-centered cubic (BCC) unit cell, was selected as a prototypical test geometry. The BCC unit cell produces a beam-based lattice structure which is mechanically robust with controllable variables (such as strut thickness, strut packing and strut angle). BCC based structures have been widely studied for different materials and 3D printing processes. Smith et al. studied two laser-sintered, BCC-based structures, made from stainless steel 316L (SS316L), for quasit-static and blast response: a conventional BCC unit cell and a modified cell with vertical beams, BCC-Z.[7] They showed that the vertical beams in the BCC-Z unit cell significantly increased the elastic modulus, yield strength, and the absorbed energy compared to the control (BCC unit cell). Also adding carbon fiber-reinforced plastic (CFRP) skins on both the top and bottom surfaces of these structures significantly increases the energy absorption density, elastic modulus, and plateau stress. Shen et al. studied the impact response of selective laser melted (SLM) lattice sandwich structures manufactured with SS316L and titanium alloy Ti 6Al4V (Ti64).[8] They found that the impact resistance was very sensitive to the unit cell geometry and SLM manufacturing parameters, and the impact resistance was improved by the increase of the lattice core density and laser energy. The mechanical behavior of BCC stainless steel micro-lattice structures manufactured by the SLM process has been studied by Gümrük et al.[9] They found that the modulus of elasticity and collapse strength of BCC structures strongly depend on the boundary conditions, and the mechanical behavior depends on the cell size, unit cell topology, and relative density. Al Rifaie et al. studied the compressive behavior of a BCC structure and its derivatives based on the vertical strut arrangements for the polymer (ABSplus-P430) manufactured via the fused deposition modeling (FDM) process.[10] They found that the BCC structure has the lowest stiffness and failure load compared with other designs that have different vertical strut arrangements. Keshavarzan et al.[11] investigated the effects of temperature, cyclic loading, and strain rate on the mechanical properties of shape memory polymer in solid, as well as DLP 3D printed Rhombic and BCC cellular structures. They found that the absorbed and the recoverable energies of the structures decrease with the increase of temperature. The residual strain and strength for Rhombic and BCC structures are approximately proportional to the applied strain rate. Rhombic structure has higher strength and stiffness compared to BCC. While most of the published works have investigated the mechanical behavior of BBC lattice structure and its derivatives for different materials and AM processes, no studies have been reported on the mechanical response of 3D-printed ETR 90 lattices of different types of unit cells and strut thickness. The aim of this work is to investigate the structural behavior including integrity of the 3D printed ETR 90 BCC lattice core sandwich structures under quasi-static and cyclic compression.

Chemical and mechanical properties of ETR 90

ETR 90 is a photoresin formulated as a one-pot, one-part photopolymer system with near-100% unreacted resin reusability at the end of the 3D printing process. ETR 90 has been tailored to reach optimum properties using a top-down-DLP system with 385 nm or 405 nm wavelengths. The ETR 90 employed in this study was black in color with a viscosity[12] of 6050 (cP) and a density[13] of 1.0306 (g/mL), each at 24°C. 3D printed ETR 90 parts exhibit an operating temperature window of − 65°C to 70°C, based on the peaks of tanδ, and a storage modulus of 51.5 MPa (at 24°C)[14] Figure 1 shows the rheological response of ETR 90 at temperature sweep from − 90 to 150°C. This profile features two well-defined peaks in tanδ (which correlate to glass transition temperatures, T_g within the system), a characteristic of well-segregated, two-phase systems. ETR 90 is uniquely tough and elastic at the same time and achieves the resulting mechanical properties through a mechanism known as photo-Polymerization-Induced-Phase-Separation (photo-PIPS).

By combining two phases with drastically different morphologies and physical properties in a thermoset material, the resulting material exhibits a unique balance of hardness, elongation at break, and ultimate strength, at levels typically seen in semi-crystalline, extrusion-processed counterparts. The mechanical properties of 3D printed ETR 90 parts (Table S1-1) and the corresponding stress–strain curves of 3D printed ETR 90 dog-bone specimens (Fig. S1-2) were shown in the Supporting Information (Section S1).

Design of sandwich lattice structures

The lattice core sandwich structures were created, with different BCC unit cells and different circular strut diameter thickness. Two specimens of each lattice structure geometry were 3D printed with the structures listed in Table I, and illustrated in Fig. 2, respectively.

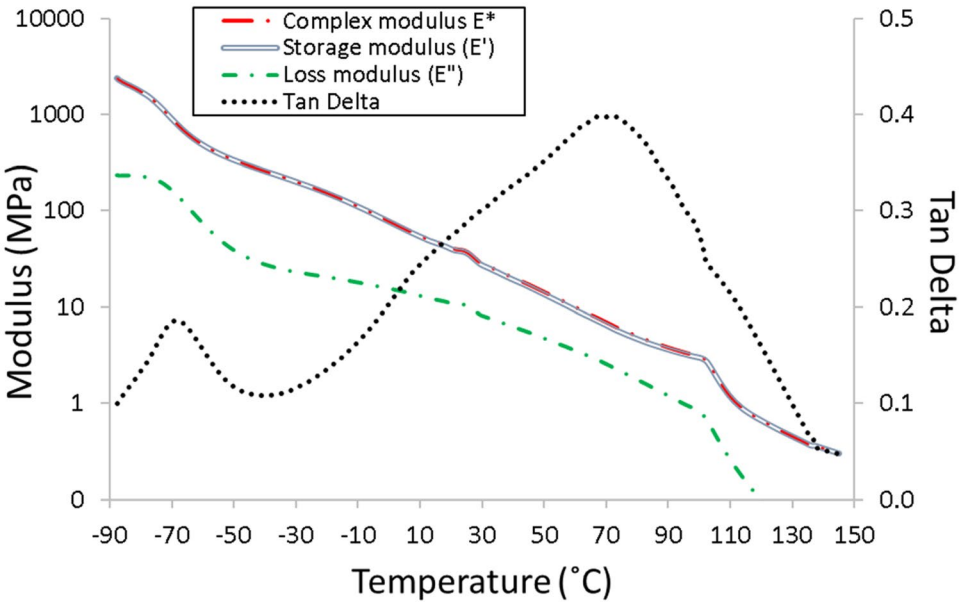

Figure 1. Dynamic mechanical analysis (DMA) of ETR 90 in tension at temperature sweep at 1.0 Hz.[15]

Table I. Summary of the characteristics of the BCC lattice structures used in this study.

Sample	Structure	Strut diameter (mm)	Cell dimensions			Sample dimensions			Skin thickness (mm)	Lattice density (V/V_0)	Mass (g)	Bulk density (g/cm^3)
			X (mm)	Y (mm)	Z (mm)	X (mm)	Y (mm)	Z (mm)				
a	BCC	1.5	5	5	5	100	100	22	1	0.29	145.87	0.66
b	BCC	2	8	8	8	96	96	22	1	0.27	93.37	0.46
c	BCC	1.5	6	6	6	96	96	22	1	0.27	93.01	0.46
d	BCC	1	5	5	5	100	100	22	1	0.19	82.31	0.37
e	BCC	1	8	8	8	96	96	22	1	0.08	48.47	0.24

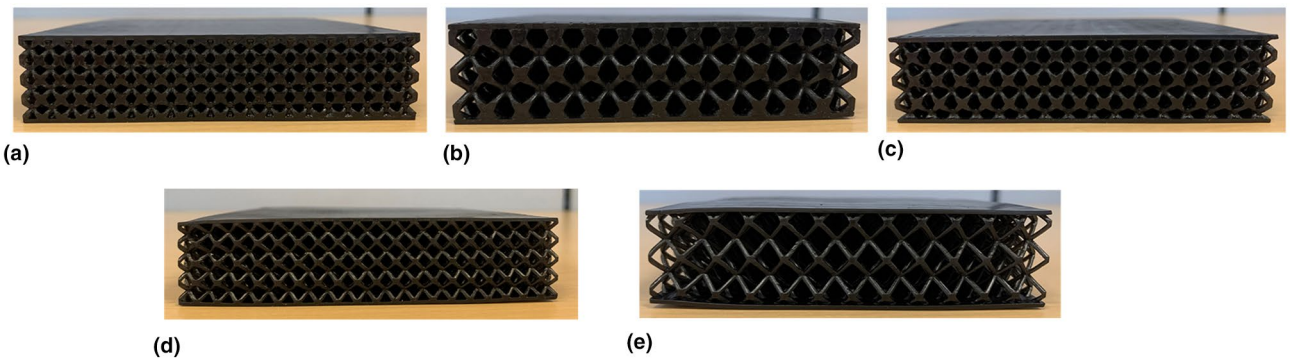

Figure 2. 3D printed ETR 90 lattice core sandwich structures.

Compression of sandwich lattice structures

Two specimens of each sample, as shown in Table I, were tested using an INSTRON 5969 universal testing system with a maximum load capacity of 50 kN. The quasi-static compression tests were performed under a crosshead speed of 12 mm/min up to 40% compression strain.[16] Pre-conditioning was performed at 1% compression strain for five cycles with a loading rate of 12 mm/min. It was observed that after three pre-conditioning cycles the behavior of samples stabilized. After pre-conditioning, one compression cycle was conducted for each specimen. The engineering effective stress–strain curves averaged among specimens for all samples and energy absorption density of the lattice structure are shown in Supporting Information Fig. S2-1 and Table S2-2, respectively. It is seen that the energy absorption density decreases with the reduction of bulk density from

samples a to e. At approximately the same bulk density, the sample with a larger strut diameter tends to provide a higher energy absorption density from results of samples b and c. For compression up to 40% compressive strain, the specific energy absorption density E (energy absorption per unit mass) follows approximately a linear relationship with bulk density, $E = A(\rho/\rho_0)$, with $A = 177.19$ mJ/g and Sample a's bulk density ρ_0.

Fatigue of the sandwich lattice structures

An all-electric material test system, INSTRON-ElectroPulsTM E10000 was used for fatigue testing of specimens of lattice structures. Two specimens of each type of lattice structure (Table I) were tested. Fatigue at 10 k cycles was conducted on these specimens. The specimens were compressed by 40% compression strain at a frequency of 1 Hz. Figure 3 shows the effective peak stress versus the number of cycles.

In Fig. 3 it is seen that the effective peak stress at the end of the 10 k cycles significantly decreases from 231 to ~ 35 MPa as the strut thickness decreases from 1.5 mm (Sample a) to 1 mm (Sample d). As the strut thickness decreases from 2 mm (Sample b) to 1 mm (Sample e) in the 8 × 8 × 8 samples, the peak stress decreases from ~ 100 to ~ 13 MPa. It is also observed that a small increase in the number of unit cells in a sample, from Sample a to Sample c, causes a reduction, (38%) in the peak stress at the end of 10 k fatigue loading cycles.

The reduction in the peak stress between the first cycle and ten thousandth cycle for all samples is observed.

The peak stress reductions are as follows: Sample a (37%), Sample b (50%), Sample c (51%), Sample d (49%), and Sample e (63%). Sample a showed the lowest reduction in the peak stress values compared with other samples.

An increase in peak stress for Sample a between cycles 5 and 95 is observed. This behavior is not typical in a homogeneous rubber material. Several factors may be inducing the phenomena. It is possible that strain induced alignment of molecules or phases, akin to the strain hardening seen in semi-crystalline thermoplastics, may be leading to this increase in peak stress. Further investigation is required for a thorough explanation.

It is seen in Table I that the total mass decreases by ~ 41% by increasing the unit cell size in a sample for the same strut thickness (i.e. Samples d and Sample e). Increase the unit cell size will decrease the number of unit cells in the lattice structure which leads to a decrease in the total mass and lattice and bulk densities.

To study the durability of 3D printed lattice structures under high fatigue cycles, only one type of specimen (Sample a as shown in Table I) was tested for 100 k loading cycles under a compression strain of 40% at frequency 1 Hz. The effective peak stress versus the number of cycles for 100 k cycles is shown in Supporting Information Fig. S3-1.

Recovery of the sandwich lattice structures

The recovery test was conducted to probe the effect of lattice structure (Sample a) on the rate of recovery. The results show that the lattice structure (Sample a) recovers 75% of the deformation in 21 s and 90% recovery in 236 s. The total recovery after 5 h was 99%. Details of experimental setup (Fig. S4-1) and measurements were explained in the Supporting Information (Section S4).

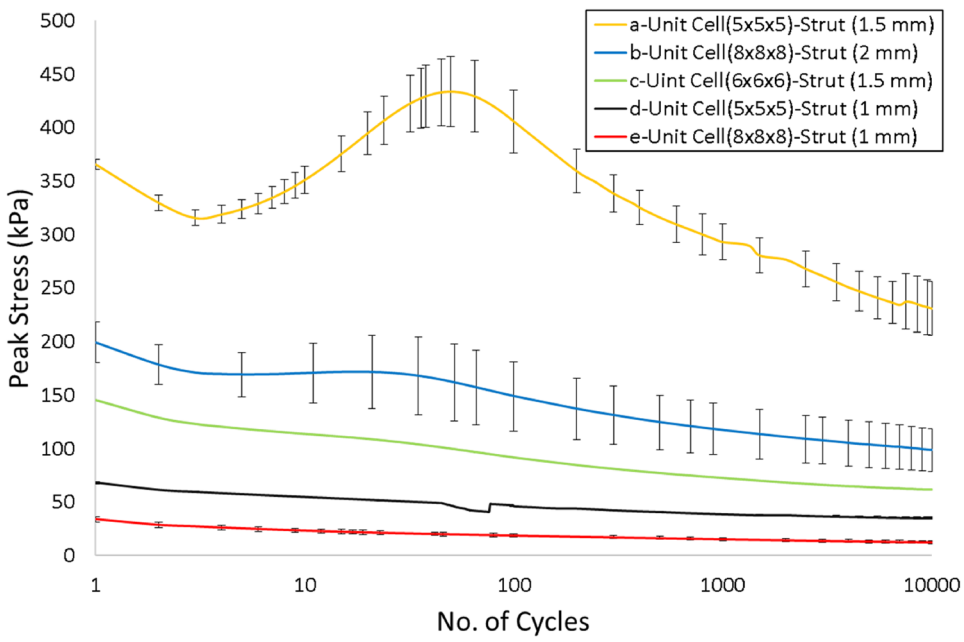

Figure 3. The effective peak stress applied on the lattice core sandwich versus the number of loading cycles.

X-ray computed tomography (CT) scan

Non-destructive X-ray CT scans were used to inspect the visually obstructed, internal struts of the 3D printed ERT90 samples to detect any damage that might have developed during cyclic fatigue. A Nikon 225 kV C1 metrology CT system, with a voxel size is 106.5 µm, was used. Detailed 3D volumetric images of the internal components of Samples a, Sample b, and Sample e are shown in Fig. S5-1. Sample a was cycled for 100 K loading cycles and Sample b and Sample e were each cycled for 10 k loading cycles, respectively. Sample a has a unit cell size of (5 × 5 × 5 mm) with a strut thickness of 1.5 mm. while Sample b and Sample e have a unit cell size of (8 × 8 × 8 mm) with strut thicknesses of 2 and 1 mm, respectively. It is observed that all lattice structures remain intact, indicating the durability of the 3D printed ETR 90 rubber lattice structures.

Discussion and conclusion

The mechanical behaviors of 3D-printed ETR 90-BCC-lattice-core-sandwich-structures were investigated under quasi-static and fatigue compression. Lattice cores with different unit cells and strut diameter were created for the sandwich with 1 mm thick face-sheets. The change of BCC strut thickness and unit cell size on the effective peak stress were characterized. All BCC lattice structures exhibit integrity in struts after fatigue (up to 100 k cycles). Excellent recovery (99%) was observed after 5 h of quasi-static compression. This study provides validity for the use of ETR 90 as a potential 3D printing rubber material for durable applications. Optimization of the topological parameters for BCC structure and comparison study between BCC and additional lattice structures will be addressed in the future work.

Acknowledgments

We thank Adaptive 3D Technologies for funding part of this effort in addition to the NSF under award numbers CMMI-1661246, CMMI-1636306, and CMMI-1726435, and the DoE award under DE-NA0003962 (subaward 1559909). We also thank foundational efforts from NIH R21 (EB020318), internal funds from the University of Texas at Dallas through the Center for Engineering Innovation and the Eugene McDermott Scholars Program and funds from DARPA award D17PC00111, NIH SPARC award 1 OT2 OD023847-01, DARPA D13AP00049 and CDMRP award W81XWH-15-1-0607. Lu is also grateful for the support by the Louis Beecherl Jr. Endowed Chair.

Supplementary information

The online version contains supplementary material available at https://doi.org/10.1557/s43579-021-00012-4.

References

1. P. Flory, *Principles of Polymer Chemistry* (Cornell University Press, Cornell, 1953).
2. M. Lukic, J. Clarke, C. Tuck, W. Whittow, G. Wells, Printability of elastomer latex for additive manufacturing or 3D printing. *J. Appl. Polym. Sci.* **133**(4), 42931 (2016). https://doi.org/10.1002/app.42931
3. P.J. Scott, V. Meenakshisundaram, M. Hegde, C.R. Kasprzak, C.R. Winkler, K.D. Feller, C.B. Williams, T.E. Long, 3D printing latex: a route to complex geometries of high molecular weight polymers. ACS Appl. Mater. Interfaces. **12**(9), 10918–10928 (2020)
4. M.F. Ashby, The properties of foams and lattices. Philos. Trans. R. Soc. A Math. Phys. Eng. Sci. **364**(1838), 15–30 (2006)
5. C. Ling, A. Cernicchi, M.D. Gilchrist, P. Cardiff, Mechanical behaviour of additively-manufactured polymeric octet-truss lattice structures under quasi-static and dynamic compressive loading. Mater. Des. **162**, 106–118 (2019)
6. K. Yu, H. Du, A. Xin, K.H. Lee, Z. Feng, S.F. Masri, Q. Wang, Healable, memorizable, and transformable lattice structures made of stiff polymers. NPG Asia Mater. **12**(1), 1–16 (2020)
7. M. Smith, W.J. Cantwell, Z. Guan, S. Tsopanos, M.D. Theobald, G.N. Nurick, G.S. Langdon, The quasi-static and blast response of steel lattice structures. J. Sandwich Struct. Mater. **13**(4), 479–501 (2011)
8. Y. Shen, W. Cantwell, R. Mines, Y. Li, Low-velocity impact performance of lattice structure core based sandwich panels. J. Compos. Mater. **48**(25), 3153–3167 (2014)
9. R. Gümrük, R.A.W. Mines, S. Karadeniz, Static mechanical behaviours of stainless steel micro-lattice structures under different loading conditions. *Mater. Sci. Eng. A* **586**, 392–406 (2013). https://doi.org/10.1016/j.msea.2013.07.070
10. M. Al Rifaie, A. Mian, R. Srinivasan, Compression behavior of three-dimensional printed polymer lattice structures. *Proc. Inst. Mech. Eng. Part L J. Mater. Des. Appl.* **233**(8), 1574–1584 (2019)
11. M. Keshavarzan, M. Kadkhodaei, F. Forooghi, An investigation into compressive responses of shape memory polymeric cellular lattice structures fabricated by vat polymerization additive manufacturing. *Polym. Test.* **91**, 106832 (2020)
12. ASTM Standard D2196-15, *Standard Test Methods for Rheological Properties of Non-Newtonian Materials by Rotational (Brookfield type) Viscometer*. ASTM International, West Conshohocken, PA (2015). https://doi.org/10.1520/D2196-15.
13. ASTM D792-13, Standard Test Methods for Density and Specific Gravity (Relative Density) of Plastics by Displacement. https://compass.astm.org/Standards/HISTORICAL/D792-13.htm. Accessed 7 Sept 2020.
14. Designation: D4065-12, Standard Practice for Plastics: Dynamic Mechanical Properties: Determination and Report of Procedures 1. https://doi.org/10.1520/D4065-12.
15. "Elastic ToughRubber™|Flexible 3D Printing|Adaptive3D." https://adaptive3d.com/additive-manufacturing/materials-used-for-additive-manufacturing/elastic-toughrubber/. Accessed 4 Sept 2020.
16. Designation: D575-91, Standard Test Methods for Rubber Properties in Compression 1. https://doi.org/10.1520/D0575-91R18.